Advances in Geo-Energy Research

Vol. 15, No. 3, p. 190-202, 2025

Original article

Novel structural design and anti-erosion performance evaluation of check valve applied to deep *in-situ* pressure-preserved coring

Xin Fang[1,2], Cong Li[1], Da Guo[1,3], Dingming Wang[1,2], Le Zhao[2], Heping Xie[1,2]*

[1]*Key Laboratory of Intelligent Construction and Healthy Operation and Maintenance of Deep Underground Engineering, Sichuan University, Chengdu 610065, P. R. China*

[2]*Guangdong Provincial Key Laboratory of Deep Earth Sciences and Geothermal Energy Exploitation and Utilization, Institute of Deep Earth Sciences and Green Energy, College of Civil and Transportation Engineering, Shenzhen University, Shenzhen 518060, P. R. China*

[3]*School of Mechanical Engineering, Sichuan University, Chengdu 610065, P. R. China*

Keywords:
Pressure-preserved coring
gas content
check valve
erosion wear
CFD-DEM coupling

Cited as:
Fang, X., Li, C., Guo, D., Wang, D., Zhao, L., Xie, H. Novel structural design and anti-erosion performance evaluation of check valve applied to deep *in-situ* pressure-preserved coring. Advances in Geo-Energy Research, 2025, 15(3): 190-202.
https://doi.org/10.46690/ager.2025.03.03

Abstract:
The pressure relief check valve plays a pivotal role in determining the oil and gas content during deep *in-situ* pressure-preserved coring. Prolonged exposure to high-pressure, high-solid-content fluids in deep wells can lead to mechanical erosion of the check valve, potentially causing severe failure and a loss of sealing integrity. To withstand the typical flow conditions in shale gas wells and on the basis of an in-depth understanding of deep fluid dynamics, a check valve was designed to operate at 70 MPa pressure and relieve pressure after coring. To mitigate erosion, a coupled Computational Fluid Dynamics-Discrete Element Method model was applied to simulate fluid flow dynamics and identify regions susceptible to erosion and wear in the valve body. The findings confirmed that the proposed check valve design meets the requirements for shale gas pressure-preserved coring and testing, with erosion mainly occurring in the constricted regions of the flow path. The erosion depth was found to increase with higher inlet flow rate and mass flow rates, demonstrating a sixfold increase as the inlet flow rate rises from 10 to 30 m/s. Non-spherical particles caused significantly more erosion than spherical ones, while the erosion depth decreased with larger particle sizes, showing a 33% reduction as particle size increased from 0.02 to 0.14 mm. To avoid sealing failures caused by prolonged erosion, the constricted flow channel was redesigned to accommodate an arc-shaped structure and appropriately widened. Simulations indicated that this structure can reduce peak pressure to 69% of the original value and minimize wall impacts. The maximum erosion depth decreased by 10%, indicating the improved durability and sealing of the redesigned check valve. These results underscore the enhanced check valve's superior erosion resistance and sealing performance, highlighting its potential for future shale gas collection and testing and providing an effective strategy to enhance the reliability and longevity of check valves.

1. Introduction

The accurate determination of the storage conditions and reserves of deep shale gas is crucial for the rational and efficient development of shale gas exploration resources in China (Xie et al., 2017; Shen et al., 2021). As shale gas development continues to accelerate, precise gas content testing has garnered increasing attention (Zhang et al., 2022; Kong

Yandy Scientific Press

*Corresponding author.
E-mail address: fangxin@stu.scu.edu.cn (X. Fang); licong@scu.edu.cn (C. Li); daguo@stu.scu.edu.cn (D. Guo); wangdingming@stu.scu.edu.cn (D. Wang); zhaole@szu.edu.cn (L. Zhao); xiehp@szu.edu.cn (H. Xie).

Received November 20, 2024; revised December 16, 2024; accepted January 5, 2025; available online January 10, 2025.

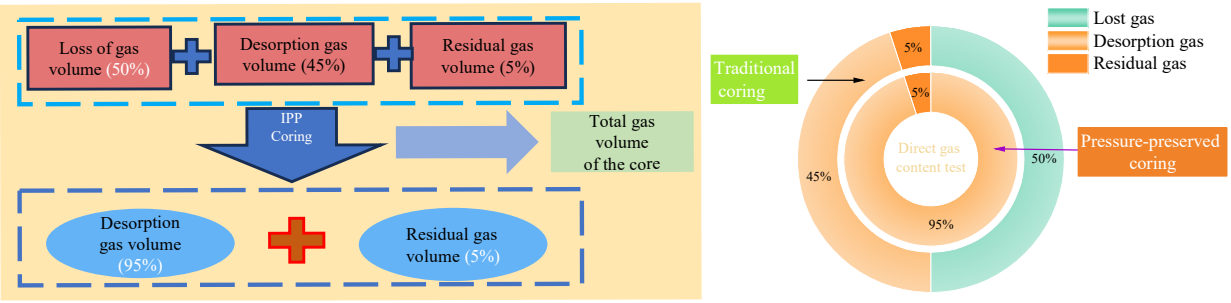

Fig. 1. Comparison between pressure-preserved coring and traditional coring methods for gas content testing.

et al., 2023). Pressure-preserved coring technology maintains *in-situ* pressure of the core and transports it to the surface by creating a sealed cavity at the bottom of the borehole (Hu et al., 2022; Fang et al., 2023). Traditional coring methods for shale gas testing rely on desorption techniques to measure gas content and use regression methods such as the USBM straight-line method, polynomial method, Smith-Williams method, and Amoco curve-fitting method to estimate lost gas content (Zhou et al., 2022). In contrast, pressure-preserved coring significantly reduces fluid loss caused by pressure fluctuations during coring and surface treatment. This approach helps prevent gas loss, as shown in Fig. 1, thereby improving the accuracy of shale gas content testing (Gao et al., 2021; Shi et al., 2024a, 2024b). As an advanced technique for preserving *in-situ* reservoir data, pressure-preserved coring is widely used in oil and gas development and has made significant progress (Abid et al., 2015; Priest et al., 2015). However, the associated pressure-preserved transfer testing technology is still underdeveloped, and accurately obtaining the fidelity parameters of pressure-preserved coring is crucial for the precise assessment of oil and gas reserves (Xie et al., 2021). Therefore, in this work, a specialized shale gas collection and testing system was developed for pressure-preserved coring, which enhances the accuracy of shale gas measurements.

A critical challenge for shale gas testing systems that utilize pressure-preserved coring is to establish a reliable, leak-proof and precise connection between the coring tube and the downstream gas collection and metering devices. To tackle this task, the development of a specialized check valve is essential, which must maintain a reliable seal under extreme downhole conditions to facilitate successful pressure-preserved coring while ensuring a secure, unidirectional connection to the surface testing equipment post-coring. Extensive research on check valves in this aspect has focused mainly on structural design. Different spool groove shapes have been explored, such as spherical, U-shaped, and triangular, to understand their effects on the flow dynamics. The results showed that spools with spherical grooves significantly increase the rate of working pressure (Ye et al., 2014). Simic and Herakovic (2015) investigated the spool inlet angle and found that a 30° angle reduces the axial force component. Furthermore, studies on spool orifice shapes have demonstrated that triangular orifices significantly mitigate flow rate fluctuations within the valve body compared to circular orifices (Lisowski and Filo, 2016). Further investigations into the internal structure, including valve seat chamfering, have provided valuable insights into the flow field distribution within the valve body (Yang et al., 2018). These studies highlight that most existing check valves rely on passive control mechanisms, where fluid flow is regulated by spring force or other external forces. However, these mechanisms are generally ineffective in controlling fluid velocity, ensuring high-pressure sealing, and most importantly, they fail to interface with the pressure-preserved coring device. Besides, they do not enable seamless connection to downstream equipment for pressure relief upon the completion of pressure-preserved coring. To overcome the above limitations, we have developed an innovative pressure relief check valve featuring a three-way channel, which integrates both the pressure relief switch and the valve body. This valve is directly connected to the center rod of the pressure-preserved coring device, ensuring a secure and stable connection between the pressure-preserved core barrel and the downstream shale gas collection and testing system. This design guarantees leak-proof, loss-free fluid collection from the core barrel. The rotary handle of the pressure relief switch facilitates a precise and easy control of fluid velocity, ensuring reliable operation. Limitations of previous studies are that, on the one hand, check valve designs to date have rarely considered the integration of the check valve with pressure-preserved coring and subsequent testing equipment; on the other hand, there has been limited focus on controlling the uniformity of fluid velocity in environments where pressure gradually decreases within the chamber. This study overcomes the technical challenge of accurately connecting the pressure-preserving coring tool to subsequent measurement equipment after coring while efficiently and precisely collecting the internal fluid from the coring barrel. By designing a specialized check valve and pressure relief switch, we could achieve stable, constant-rate fluid collection. This prevents issues related to excessive depressurization rates or sudden pressure increases, which would otherwise cause downstream measurement equipment to fail, leading to fluid leakage and test failure.

The complex downhole fluid environment introduces a large number of solid particles into the collected shale gas (Liu et al., 2023). As the gas flows through the check valve, these particles gain kinetic energy and in turn potentially erode critical components, leading to valve malfunctions, seal failure, and a reduced component lifespan. Therefore, predicting fluid movement and particle erosion patterns within the valve is cru-

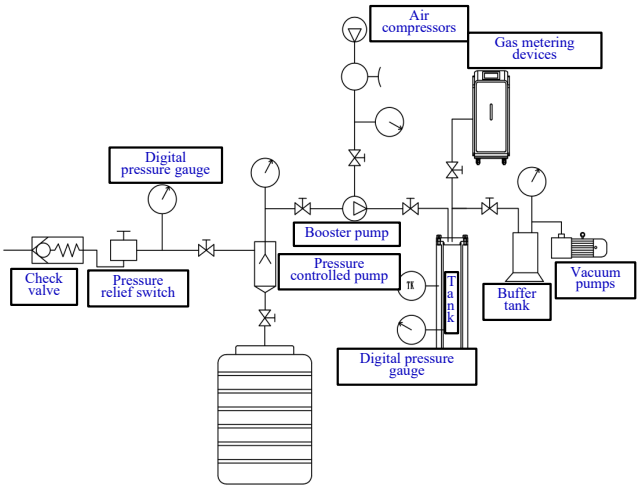

Fig. 2. On-site pressure relief gathering process based on pressure-preserved coring.

cial for preventing such damage. Erosion is a significant and complex phenomenon, which has been studied experimentally by scholars for many years (Fry et al., 2017). Computational fluid dynamics (CFD) is an effective tool for analyzing flow characteristics in various fluid structures (Alghurabi et al., 2021; Quan et al., 2022; Guo et al., 2023) and has been increasingly used to simulate interactions between solid particles and fluid flow. Some researchers have applied CFD to study particle erosion and the abrasion of structures (Domagała et al., 2018), while others have developed MATLAB or Python-based models to track particle trajectories and predict the resulting erosion and wear (Yin et al., 2017). These studies are crucial for predicting the erosion and wear of pipelines, pressure components and fluid equipment. However, CFD-based erosion studies still have limitations, as they treat the fluid and solid phases as a single system, both considered as Eulerian phases. This approach overlooks interactions between the two phases as well as factors like particle shape, particle collisions, and interactions between particles and the wall. Notably, particle collisions and shape play a key role in erosion wear (Xu et al., 2016). Therefore, a more accurate simulation method is needed to predict and analyze the erosion phenomenon in check valves.

In order to address the diverse requirements of shale gas gathering and testing systems based on pressure-preserved coring-including reliable sealing in high-temperature, high-pressure environments, precise control of fluid velocity, and accurate, leak-free integration with both the coring system and downstream measurement devices-a special pressure relief check valve has been developed. In response to the limitations of existing CFD erosion models and the need for more in-depth erosion studies of newly developed check valves, this study utilized the CFD-DEM coupling method to conduct a more precise erosion analysis of the check valve, which takes into account both the particle movement state and particle shape, incorporating the Archard wear model to investigate internal fluid flow as well as erosion and wear. Furthermore, it examined the particle flow dynamics and erosion-wear patterns under different inlet velocities, particle shapes and mass loads. Compared with traditional CFD erosion studies, the CFD-DEM coupling method provides more accurate and reliable results. In addition, to prevent sealing failure caused by prolonged erosion, key structures of the valve body were optimized to enhance erosion resistance. The modified valve has been tested and verified in field applications.

2. Pressure relief check valve development

A shale gas collection and testing system based on pressure-preserved coring technology can significantly enhance the accuracy of shale gas measurements, thereby it is of great importance for shale exploration and development and the evaluation of shale reservoir reserves. Our team has developed a specialized shale gas collection and testing system designed to interface with pressure-preserved coring equipment, as shown in Fig. 2. This system can be directly connected to the pressure-preserved coring device and, after depressurization and gas-liquid separation, enable the collection of fluid from the core and accurate gas content determination under constant-temperature conditions. Since pressure-preserved coring contains high-pressure gas and the coring device is designed to withstand pressures up to 70 MPa, it is essential to depressurize the gas before it enters subsequent testing equipment. Therefore, a pressure relief check valve needs to be installed between the pressure-preserved coring device and the downstream gas metering equipment. This valve must ensure a precise, sealed connection between the pressure-preserved coring device and the shale gas collection and testing system, with a pressure resistance of at least 70 MPa, and be capable of efficiently venting gas under various complex operating conditions.

In order to tackle the above tasks, we have developed a check valve specifically designed for pressure-preserved coring and shale gas collection and testing systems, as shown in Fig. 3. The check valve consists of two primary components: a pressure relief switch and the check valve body. The pressure relief switch is composed of a switch body, an ejector pin and a rotating handle. The switch body contains a tee channel, with the ejector pin vertically mounted in the first channel and connected to the switch body via a threaded joint. The check valve is securely fastened to the center rod of the corer using internal threads. The upper end of the ejector pin is linked to the rotating handle, enabling the pin to move up and down relative to the switch body via the rotation of the handle. The lower end of the ejector pin interfaces directly with the spool of the check valve, as illustrated in Fig. 3(a). The check valve itself comprises a valve body, a valve stem, a valve spool, and a reset spring, all housed within the valve body. The lower end of the valve stem is connected to the valve spool, while the upper end interfaces with the lower end of the ejector pin. The valve spool and valve body operate via vertical sliding, with complementary sealing surfaces. A reset spring applies axial force to maintain contact between these surfaces. When an external force pushes the valve stem and spool downward, the sealing surfaces separate, thereby opening the check valve, as shown in Fig. 3(b). This specially engineered check valve is integrated into the center rod of the pressure-preserved coring

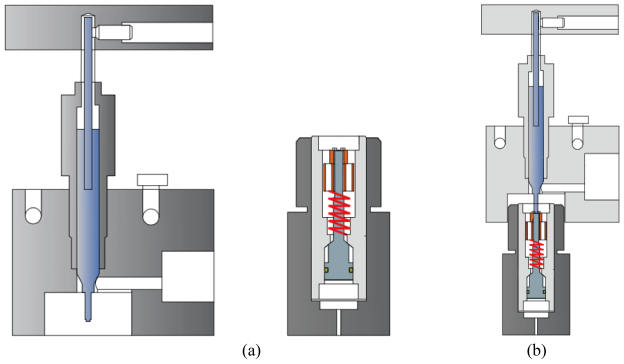

Fig. 3. Designed (a) check valves Pressure relief switches and (b) check valves Cooperative relationship.

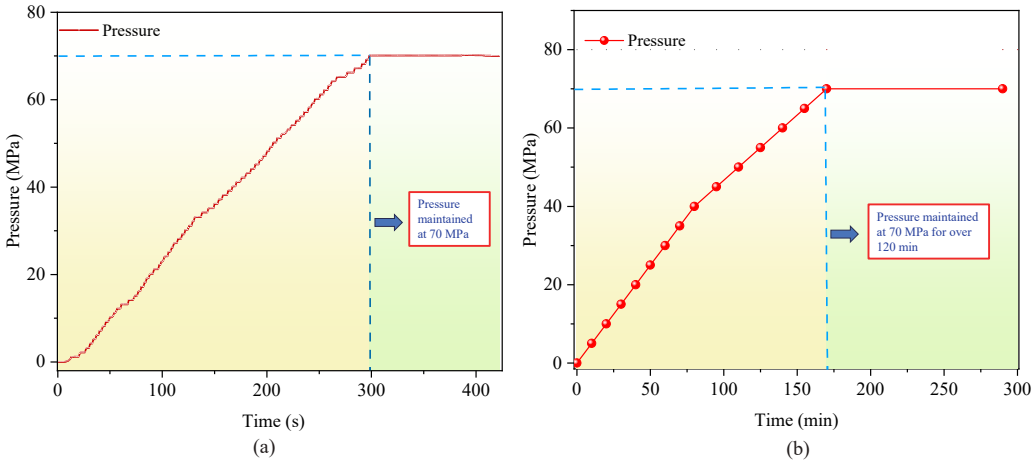

Fig. 4. Check valve pressurization curves of (a) laboratory pressurization curve and (b) connected corer field pressure test curve.

system, establishing a connection between the medium channel of the valve body and the pressure relief hole of the center rod.

The designed check valve can maintain a seal under a pressure environment of 70 MPa at depth, ensuring successful pressure-preserved coring. To verify the sealing ability of the check valve, we designed a pressure testing device in the laboratory, installed the check valve in this device, and subsequently conducted pressure tests. From the pressure curve during the test, as shown in Fig. 4(a), it can be seen that the check valve can withstand a pressure of 70 MPa and maintain this pressure stably.

Previous pressure tests, which were conducted using indoor assembly pressure equipment for a relatively short duration, could not accurately replicate actual pressure conditions encountered in the field. Besides, the check valve was not installed in the corer during the initial test. Therefore, it was considered necessary to install the check valve in the corer and perform another pressure test at 70 MPa. The pressurization test on the corer was carried out using the JT4DSY-20/80 pump from Sichuan JITE Machinery Co., Ltd. Due to the condition of high pressure in the experiment, comprehensive safety precautions were implemented: a high pressure resistant glass cover was placed around the corer and a remote operating system was developed. To further ensure safety, the pump switch was relocated 50 meters away and connected by cables. Furthermore, a camera was positioned next to the pressure gauge to monitor real-time pressure fluctuations. During the test, the pressure was gradually increased by 5 MPa every ten minutes until it reached 70 MPa, after which the pressure was stabilized. The recorded test results are shown in Fig. 4(b). Once the check valve was installed in the corer, the pressurization process was continued without any leakage. The pressure in the coring assembly was maintained at 70 MPa for approximately two hours with minimal leakage. Based on both the laboratory and coring assembly test results, the designed check valve exhibited excellent sealing stability at 70 MPa, demonstrating superior pressure-preservation capability that meets the stringent requirements of deep oil and gas exploration.

The above experimental results indicate that the proposed check valve design meets the pressure-preservation coring requirements for deep oil and gas wells: It ensures a precise connection between the corer and subsequent measurement equipment upon the competion of coring, enabling gas metering and fluid collection.

3. Numerical simulation of erosion

3.1 Theoretical modeling

During coring in shale gas formations, the core barrel fills with gas and when the check valve opens, gas escapes, forming a solid-liquid two-phase flow. Compared to traditional CFD

models that focus solely on fluid flow, this study employs a coupled CFD-DEM approach to simulate the erosion caused by sand-laden fluids in shale gas check valves. The bidirectional coupling method considers the interactions between the fluid and particles (Farokhipour et al., 2019). In the simulation of this study, conducted using FLUENT and EDEM software, fluid-particle, particle-fluid, particle-particle and particle-wall interactions are fully accounted for and the Archard wear model is employed to calculate erosion. The model framework consists of three main components (Zhu et al., 2007; Duarte et al., 2016).

3.1.1 Fluid flow modeling

During the check valve relief operation, shale gas flows through the valve body as a continuous phase, governed by continuity and momentum equations, which differ in single-phase and bidirectional coupling. CFD-DEM simulations often use one-way coupling to reduce the computational cost, neglecting particle-induced forces on the fluid. Bidirectional coupling accounts for these forces, crucial for accurate fluid motion modeling. The governing equations are as follows (Chen et al., 2015):

$$\frac{\partial}{\partial t}\left(\alpha_f \rho_f\right)+\frac{\partial}{\partial x_j}\left(\alpha_f \rho_f u_j\right) a=0 \tag{1}$$

The momentum equation is:

$$\begin{aligned}&\frac{\partial}{\partial t}\left(\alpha_f \rho_f u_i\right)+\frac{\partial}{\partial x_j}\left(\alpha_f \rho_f u_i u_j\right)\\&=-\frac{\partial p}{\partial x_i}+\frac{\partial}{\partial x_j}\left[\alpha_f \mu_{\text{eff}}\left(\frac{\partial u_i}{\partial x_j}+\frac{\partial u_j}{\partial x_i}\right)\right]+\alpha_f \rho_f g+\vec{S}_{\text{mon}}\end{aligned} \tag{2}$$

In this context, ρ_f represents fluid density, u is the fluid velocity, p represents mean fluid pressure, μ_{eff} is the fluid's effective viscosity, and S_{mon} denotes the momentum transfer source term from the solid to the continuous phase, whose calculation is as follows:

$$\vec{S}_{\text{mon}}=\frac{-\sum(\vec{F}_D+\vec{F}_B+\vec{F}_L)}{V_{\text{cell}}} \tag{3}$$

In this context, drag $\vec{F}_D$, buoyancy $\vec{F}_B$ and lift forces $\vec{F}_L$ are included, with detailed explanations in later sections. V_{cell} represents the fluid dynamic unit volume and α_f denotes the particle-adjacent porosity, which is calculated as follows:

$$\alpha_f=1-\frac{\sum_{i=1}^{n} V_{p,i}}{V_{\text{cell}}} \tag{4}$$

where $V_{p,i}$ denotes the volume of particle i in the selected CFD cell, n represents the number of particles in the cell, and V_{cell} means the volume of the cell.

3.1.2 Discrete phase modeling

The trajectory of particles in the fluid during pressure relief by the check valve can be determined by solving motion equations in the Lagrangian framework on the basis of the following equilibrium equations (Farokhipour et al., 2019; Yang et al., 2021):

$$\begin{aligned}m_P\frac{\mathrm{d}\vec{u}_P}{\mathrm{d}t}&=\vec{F}_{\mathrm{g}}+\vec{F}_D+\vec{F}_{LS}+\vec{F}_{LR}+\vec{F}_B+\vec{F}_{IC}\\I_P\frac{\mathrm{d}\vec{\omega}_P}{\mathrm{d}t}&=\vec{T}_{\mathrm{c}}+\vec{T}_{\mathrm{f}}\end{aligned} \tag{5}$$

where $\vec{u_p}$ represents the particle velocity vector, F_g denotes gravity, $\vec{F_D}$ denotes fluid drag, $\vec{F_{LS}}$ refers to Saffman lift, $\vec{F_{LR}}$ denotes Magnus lift, $\vec{F_B}$ denotes buoyancy, $\vec{F_{IC}}$ corresponds to the collision force applied on the particle, T_{c} denotes the torque arising from inter-particle contact forces, T_{f} corresponds to the torque exerted by fluid on the particle, $\vec{\omega}_P$ is the particle's angular velocity, $I_P=0.1m_P d_P^2$ represents the spherical particle's mass moment of inertia, and d_P is the particle diameter. The calculations for each term on the right-hand side are detailed as follows (Farokhipour et al., 2019):

The expression for the fluid drag force $\vec{F_D}$ is given as (Haider and Levenspiel, 1989):

$$\vec{F}_D=C_D\rho\frac{\pi d_p^2}{8}\left|\vec{u}-\vec{u_p}\right|\left(\vec{u}-\vec{u_p}\right) \tag{6}$$

where $\vec{u}$ is the instantaneous fluid velocity vector that can be written as the sum of the mean flow velocity and turbulent velocity fluctuations and C_D is the drag coefficient and is expressed as (Haider and Levenspiel, 1989):

$$C_D=\frac{24}{\mathrm{Re}_P}\left(1+b_1\mathrm{Re}_P^{b_2}\right)+\frac{b_3\mathrm{Re}_P}{b_4+\mathrm{Re}_P} \tag{7}$$

The empirical parameters are defined as:

$$b_1=0.1862, b_2=0.6529, b_3=0.4373, b_4=7,185.4 \tag{8}$$

Re_p represents the particle Reynolds number, which is calculated as:

$$\mathrm{Re}_P=\frac{\rho\left|\vec{u}_P-\vec{u}\right|d_p}{\mu} \tag{9}$$

The slip shear lift force, also referred to as Saffman lift, is computed using the following formula (Farokhipour et al., 2019):

$$\vec{F}_{LS}=1.615d_P^2(\rho\mu)^{\frac{1}{2}}\left(\frac{1}{|\vec{\omega}_P|}\right)^{0.5}C_{LS}\left[\left(\vec{u}-\vec{u}_p\right)\times\vec{\omega}\right] \tag{10}$$

where $\vec{\omega}=0.5(\nabla\times\vec{u})$ denotes the rotation of the fluid and C_{LS} is the Saffman lift coefficient, which is defined as:

$$C_{LS}=\begin{cases}(1-0.3314\beta^{\frac{1}{2}})e^{-\left(\frac{\mathrm{Re}_P}{10}\right)}, & \mathrm{Re}_P\le 40\\0.0524(\beta\mathrm{Re}_P)^{\frac{1}{2}}, & \mathrm{Re}_P>40\end{cases} \tag{11}$$

The Magnus lift force, arising from particle rotation, is calculated as follows (Oesterlé and Dinh, 1998):

$$\vec{F}_{LM}=\frac{\pi\rho d_p^2}{8}C_{LM}|\vec{u}_p-\vec{u}|\frac{\vec{\Omega}\times(\vec{u}-\vec{u}_p)}{|\vec{\Omega}|} \tag{12}$$

where C_{LM} is the Magnus lift coefficient, which is defined by:

$$C_{LM}=0.45+\left(\frac{\mathrm{Re}_r}{\mathrm{Re}_p}-0.45\right)e^{-0.05684\mathrm{Re}_r^{0.4}\mathrm{Re}_p^{0.3}} \tag{13}$$

The buoyancy force is determined according to Archimedes' principle:

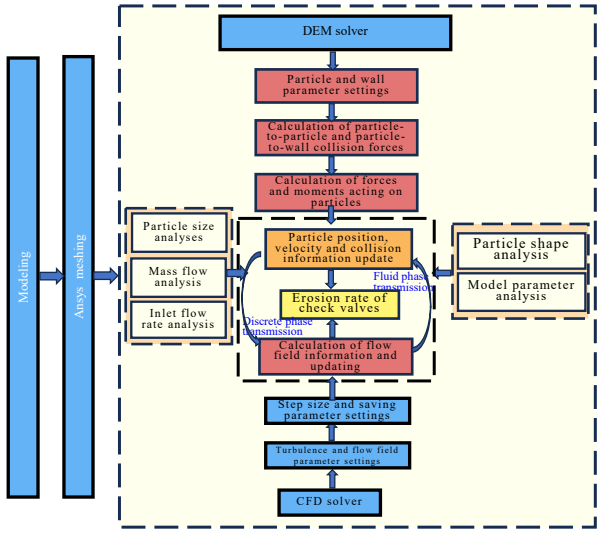

Fig. 5. CFD-EDM coupling principle.

$$F_B = \frac{\pi}{6} d_p^3 (\rho_f - \rho_p) g \tag{14}$$

where ρ_f is fluid density and ρ_p is particle density.

3.1.3 Erosion modeling

Erosive wear occurs when fluid-carried particles strike a surface at specific velocities and angles, causing material loss and craters. The extent of wear on metal surfaces is mainly influenced by the impact angle and particle velocity (Zhang et al., 2007). While the erosion rate has been traditionally used to quantify wear severity, it does not provide a clear indication of material erosion or the specific wear mechanisms. This study uses the erosive wear model proposed by Archard (1953), which quantifies wear by the volume of material removed Q, influenced by factors like material hardness and applied load. This semi-empirical model expresses wear as the erosion depth per unit area, denoted as h:

$$Q = \frac{K}{H} F_n d_s \tag{15}$$

$$h = \frac{Q}{A} \tag{16}$$

where Q represents the volume of the eroded material (mm^3), K is the wear constant, H denotes the hardness value of the material surface $N{\cdot}mm^{-2}$, ds is the sliding distance (mm), F_n stands for the force point load (N), A is the contact area between the particle and the wall (mm^2), and h is the wear depth per unit area (mm).

3.2 Numerical simulation of erosion

3.2.1 Coupling process

The coupling of Computational Fluid Dynamics (CFD) and Discrete Element Method (DEM) calculates particle and gas motion in a gas-solid two-phase flow, facilitating the exchange of momentum and energy between the phases. In this research, to conduct a simulation study on check valve erosion, we leverage the CFD module in ANSYS FLUENT coupled with EDEM. By employing the Eulerian-Lagrangian coupled model, CFD-DEM adeptly captures fluid-particle interactions. The transient bidirectional data transfer characterizing the coupling process involves CFD calculating flow field information for one time step, subsequently initiating DEM for a corresponding iteration. Fluid motion information is communicated to EDEM through the coupling interface, impacting particle motion. Subsequently, particle information is fed back into CFD, influencing the fluid. The transient simulation unfolds via a systematic loop iteration. The illustrated Fig. 5 encapsulates the orchestrated flow of the coupled simulation.

3.2.2 Modeling and Setting of Parameters

Using a three-dimensional modeling software, we can accurately depict the check valve in Fig. 6(a). The model is simplified and imported into ANSYS for meticulous mesh delineation. The configurations for the inlet and outlet surfaces and wall boundaries are precisely defined using a multi-area mesh delineation method. The key delicate components are encrypted. Considering the actual operational conditions, the particle size d ranges from 0.02 to 0.14 mm and the inlet flow rate v varies between 10 and 30 m/s, consistent with actual working conditions.

According to the flow characteristics and configuration of the designed check valve, the fluid domain within the check valve was extracted using the ANSYS pre-processing module, and the corresponding three-dimensional computational domain was established. This fluid model was imported into ANSYS software for meshing, employing a multi-area unstructured hexahedral mesh and encrypting the critical parts. The meshing results and boundary conditions were set, as shown in Fig. 6(b). The fluid within the domain was natural gas, characterized by a density of 0.762 kg/m^3, a viscosity of 6×10^{-5} Pa·s, a gas velocity ranging from 10 to 30 m/s, a particle density of 2650 kg/m^3, a particle diameter between 0.03 and 0.15 mm, and a particle mass flow rate ranging from 0.0001 to 0.01 $kg{\cdot}s^{-1}$ (Lyu et al., 2023). Internal sand particles were automatically generated by utilizing the particle factory in EDEM.

Numerous studies have emphasized the influence of mesh quantity on calculation outcomes, highlighting the necessity of mesh-independence verification. In this study, mesh refinement was performed for the computational domain, as depicted in Fig. 6(b). For CFD-DEM coupling, it is crucial to maintain a mesh size three times larger than the particle size. Sensitivity analyses were conducted on the fluid domain grid with a mass flow rate of 0.0005 kg/s, an inlet velocity of 20 m/s, and a particle size of 0.05 mm. This study utilized the maximum erosion depth as an evaluation index and tested five sets of grid resolutions: 89,000, 102,044, 142,453, 181,325, and 239,004 cells. The results shown in Fig. 7 indicate that the maximum erosion depth stabilizes when the number of grid cells exceeds 181,325. Therefore, for optimized computational efficiency, a grid configuration of 181,325 cells was selected for the numerical investigation.

The Hertz-Mindlin (no-slip) model was chosen as the contact model between particles or between particles and walls in EDEM. The principle of this collision model is shown in Fig. 8.

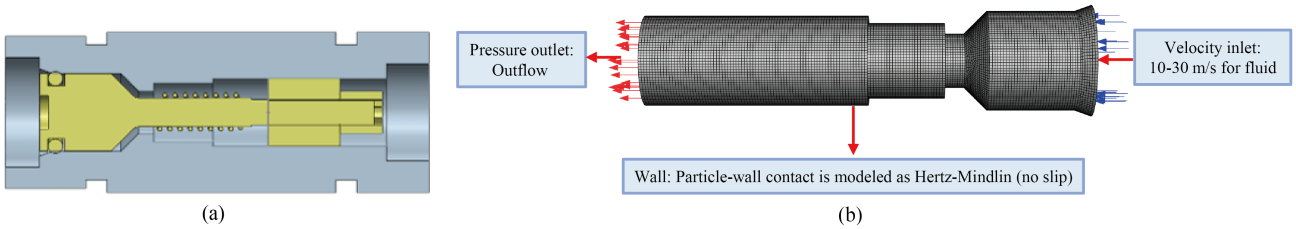

Fig. 6. Model building and meshing (a) design check valve modeling and (b) fluid domain boundary conditions and meshing.

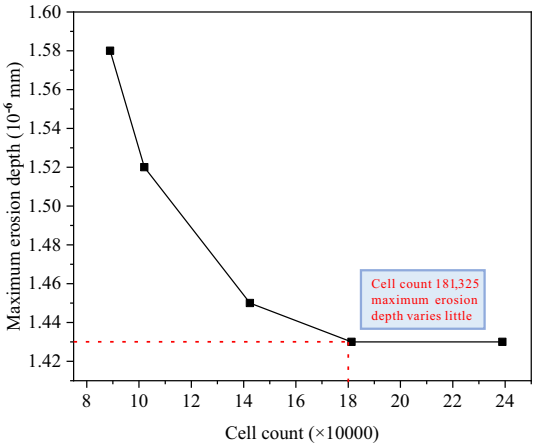

Fig. 7. Grid-independent verification of erosion depth.

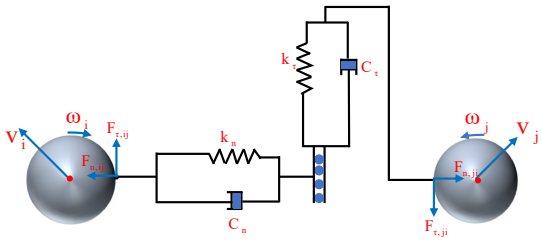

Fig. 8. Hertz-Mindlin model.

Fig. 8 illustrates the collision model, where each collision force or moment is conceptualized as a linear elastic-damped model, akin to a spring-damper system. This model succinctly and efficiently represents the force changes during particle collisions, ensuring an accurate simulation of particle system dynamics. On the basis of material properties, wear coefficients of 10-12 were selected. Other parameters were configured as follows: Particle density of 2,650 kg/m^3, particle Poisson's ratio of 0.4, and particle shear modulus of 88 MPa. The check valve material was 2205 stainless steel, a high-strength alloy commonly used in high-pressure pipelines. Its parameters are as follows: Density of 7.98×10^3 kg/m^3, elastic modulus of 190 GPa, tensile strength exceeding 616 MPa, yield strength of 587 MPa, and Brinell hardness less than 187 HB. The Poisson's ratio is 0.286. Additional parameters included a particle-particle static friction factor of 0.44, a particle-particle kinetic friction factor of 0.27, a particle-particle coefficient of restitution of 0.01, a particle-tubing static friction factor of 0.50, a particle-tubing kinetic friction factor of 0.15, and a particle-tubing coefficient of restitution of 0.01. The total simulation time was set to 1 second.

4. Results and discussion

4.1 Analysis of simulation results

The foundation of erosion simulation lies in the calculation of the flow field, where the flow characteristics of the internal gas source play a crucial role in influencing the erosion and wear of the valve body wall. In this study, simulations were conducted based on the actual operating conditions of the check valve, with a gas flow rate of 20 m/s, particle diameter of 0.05 mm, and a particle mass flow rate of 0.0005 kg/s. Fig. 9 presents the pressure and velocity distributions inside the designed check valve under these operating conditions, where Fig. 9(a) illustrates the fluid pressure distribution. It is evident that the pressure is the highest when the fluid initially enters the valve body and gradually decreases as it flows through. However, a negative pressure zone is observed in the region where the flow channel suddenly narrows. This phenomenon is attributed to the abrupt constriction of the flow channel, which, influenced by centrifugal forces and the bending of flow lines, leads to the contraction of the inner fluid while the outer fluid diffuses. The centrifugal force exerted on the outer wall of the check valve generates traction, thereby reducing the wall pressure. This pressure reduction converts the specific pressure energy on the outer side of the valve into the kinetic energy of the fluid, resulting in an increase in flow velocity and the formation of a negative pressure zone. The velocity distribution of the fluid is shown in Fig. 9(b). It can be observed that the fluid enters from the inlet end with a uniform velocity distribution, perpendicular to the inlet cross-section. As the fluid moves into the constricted region of the internal runner, which corresponds to the negative pressure zone in Fig. 9(a), it undergoes a sudden contraction, altering the flow direction and causing a sharp increase in velocity.

The distribution of erosive wear on the inner wall of the check valve is illustrated in Fig. 10(a). Erosive wear primarily occurs in the narrowing region of the fluid flow path along the valve body wall, exhibiting a circular and uneven pattern. As the fluid enters the valve body, its velocity is perpendicular to the inlet cross-section. Upon reaching region I in Fig. 10(a), the change in velocity direction causes solid particles to collide with the wall, initiating the erosion process. When the fluid enters the narrowing section of the flow channel and the flow line bends in region II of Fig. 10(a), corresponding to the negative pressure zone in Fig. 9(a), and the velocity of fluid increases significantly, carrying solid particles at higher speeds. These conditions intensify both the frequency and impact strength of particle collisions, enhancing the cutting

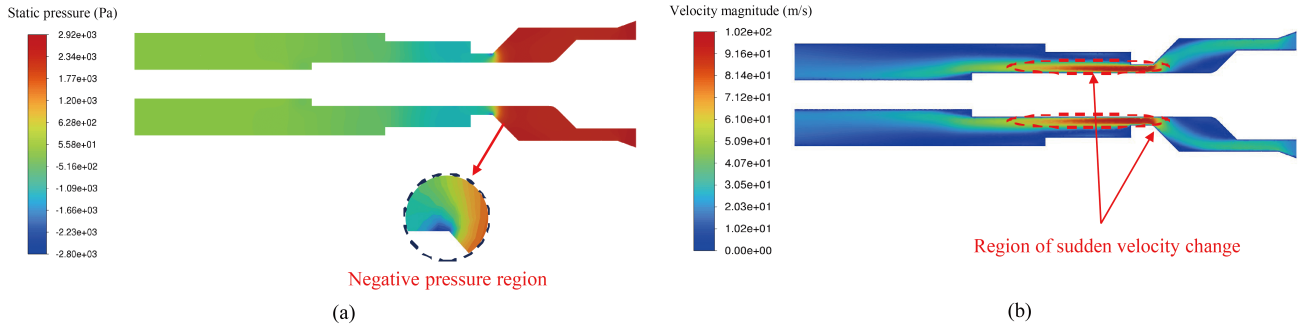

Fig. 9. Fluid pressure and velocity distribution of (a) pressure distribution and (b) velocity distribution.

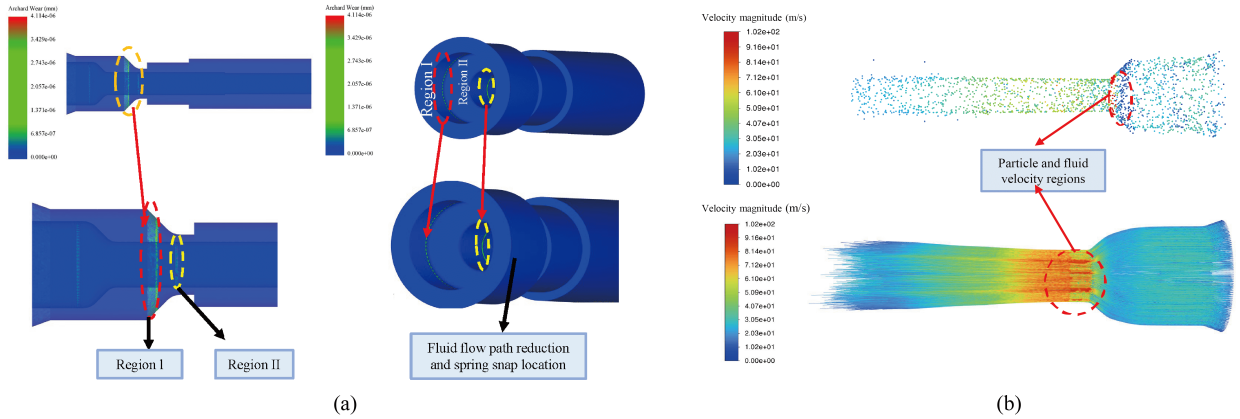

Fig. 10. Valve body erosion result (a) Check valve surface erosion (b) Particle velocity distribution and particle trajectory.

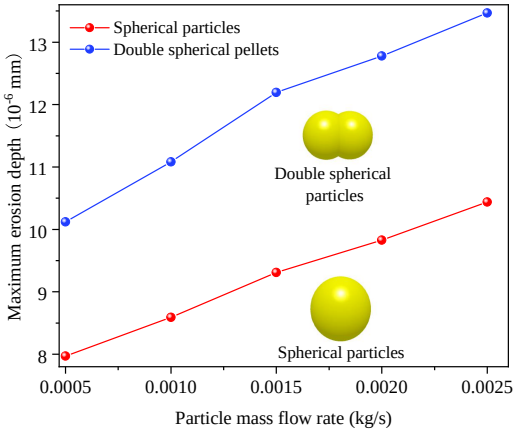

Fig. 11. Effect of particle shape on maximum erosion depth.

effect on the wall and thereby accelerating the erosion and wear process. Consequently, a more pronounced maximum erosion depth is observed in this area. This phenomenon further demonstrates the close association between fluid flow conditions and particle-induced erosion.

The internal particle trajectories are shown in Fig. 10(b) . It can be observed that the particles carried by the fluid experience a significant increase in velocity when they enter the region where the fluid flow channel suddenly narrows, as marked in Fig. 10(b). This corresponds to the areas of erosion and wear identified in Fig. 10(a), as well as to the negative pressure zone and the location of sudden velocity increase in Fig. 9. This phenomenon occurs because particles enter from the horizontal direction, and due to the sudden narrowing of the flow channel and the corresponding increase in fluid velocity, the particle velocity also increases. The particles directly impact the valve body wall, causing intense collisions and significant wall damage, which further exacerbates the erosion process. After striking the valve wall, the particles are carried by the high-speed fluid along the flow path and eventually exit through the outlet.

A key advantage of the coupled CFD-DEM approach utilized in this study lies in its ability to determine the influence of particle shape on the erosive wear of check valves using EDEM software. In this research, both spherical and double-spherical particles were selected to study the erosion behavior of check valves. To ensure the accuracy and reliability of the results, the key physico-mechanical parameters-such as particle density, volume, and mass-were held constant, with particle shape being the sole variable. The erosion behavior of different particle shapes under varying mass flow rates is presented in Fig. 11. The findings show that, with an increase in mass flow rate, erosion depth also increases, although the rate of increase gradually diminishes. Notably, the erosion induced by non-spherical particles is found to be significantly greater than that caused by spherical particles. These results underscore the substantial impact of particle shape on the erosive wear of components.

4.2 Influence of particle mass flow rate

The particle mass flow rate plays a critical role in the erosion of check valves. In actual oil and gas coring operations, the working conditions are highly complex, and variations in

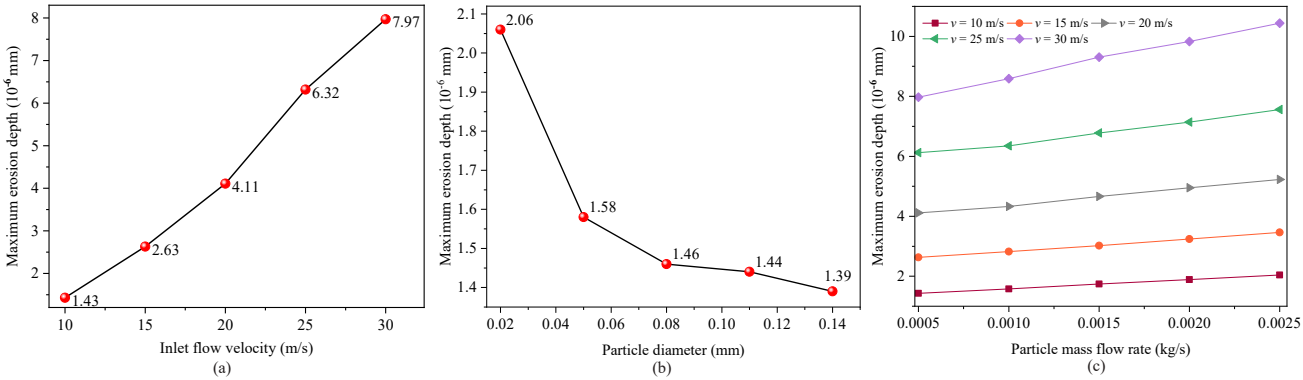

Fig. 12. Influence curve of (a) inlet flow velcity, (b) particle diameter and (c) prticle mass flow rate at different inlet flow velcity.

coring types and operational environments contribute to differing particle concentrations within pressure-preserved core barrels. During pressure release and gas collection, these differences inevitably lead to variations in the particle mass flow rates. Consequently, to better address the challenges posed by various coring environments and coring types, it is crucial to investigate the influence of particle mass flow rate on check valve erosion. In this study, particle mass flow rates were set as 0.0005, 0.001, 0.0015, 0.002, and 0.0025 kg/s, while inlet flow velocities were configured as 10, 15, 20, 25, and 30m/s, with a fixed particle size of 0.05 mm. By performing comprehensive simulations, the erosion behavior of the check valve was analyzed and the relationship between particle mass flow rate and maximum erosion depth at different inlet flow velocities was established, as depicted in Fig. 12. From the plotted curves, it is evident that, for all inlet flow velocities, the maximum erosion depth increases significantly with rising particle mass flow rates, and this trend is more pronounced at higher mass flow rates. To further elucidate the relationship between erosion depth and inlet velocity, the maximum erosion depth for a particle mass flow rate of 0.0005 kg/s as a relation of inlet velocity is presented in Fig. 12(a). The results indicate a clear upward trend in maximum erosion depth as the inlet velocity increases. Specifically, when the inlet velocity rises from 10 to 30 m/s, the erosion depth is observed to increase by a factor of six. This phenomenon can be explained by the fact that, as the inlet velocity increases, particle velocity within the fluid also rises after undergoing fluid dynamics calculations in FLUENT and subsequent transfer to EDEM. This velocity increase translates to the greater kinetic energy of the particles. When the flow reaches the check valve and passes through regions of flow constriction, the particles undergo intensified collisions with the valve wall. The increased inlet velocity amplifies both the collision frequency and intensity, thereby exacerbating erosion. Additionally, at a fixed inlet velocity, an increase in particle mass flow rate results in a higher number of particles colliding with the valve within the same time frame, increasing the frequency of collisions and intensifying the erosive effect, ultimately resulting in a greater wear of the check valve. Fig. 13 illustrates the erosion contour maps of the valve at different mass flow rates, which exhibit the same trend.

4.3 Influence of particle size

The coring environment in oil and gas fields is inherently complex, with variations in lithology and site conditions leading to differences in particle size within the core barrel during each coring operation. As a result, it is essential to investigate the impact of varying particle sizes on the erosion and wear of check valves. In this study, a fixed mass flow rate of 0.001 kg/s was maintained, with inlet velocities set at 10, 15, 20, 25, and 30 m/s. The particle sizes were varied at 0.02, 0.05, 0.08, 0.11, and 0.14 mm. The corresponding changes in the maximum erosion depth, as influenced by increasing particle size at different inlet velocities, were calculated and presented in Fig. 14, accompanied by the erosion cloud diagrams. The results show that, at the same velocity level, as the particle size increases, the maximum erosion depth decreases. When the particle size increases from 0.02 to 0.08 mm, the erosion depth significantly decreases, with the largest reduction reaching up to 30%. However, when the particle size exceeds 0.08 mm, the rate of decrease in erosion depth slows, and there is almost no further reduction. Overall, as the particle size increases from 0.02 to 0.14 mm, the erosion depth decreases by 33%. This phenomenon is mainly attributed to the increase in particle size, leading to a proportional increase in particle mass. At a constant inlet velocity, the gas-carrying capacity decreases, leading to a reduction in the number of particles carried at the same velocity. The particle velocity decreases, resulting in a reduction in kinetic energy, which weakens the ability of the particles to impact the check valve wall, thereby reducing the erosion depth of the valve. It can also be observed that, with an increase in inlet velocity, the reduction in the maximum erosion depth becomes more significant for the same increment in particle size. This can be attributed to the fact that higher velocities carry a greater number of particles, which leads to an increase in the particle scale. Consequently, the larger particle size results in a more pronounced decrease in the number of transported particles, thereby enhancing the reduction in erosion depth.

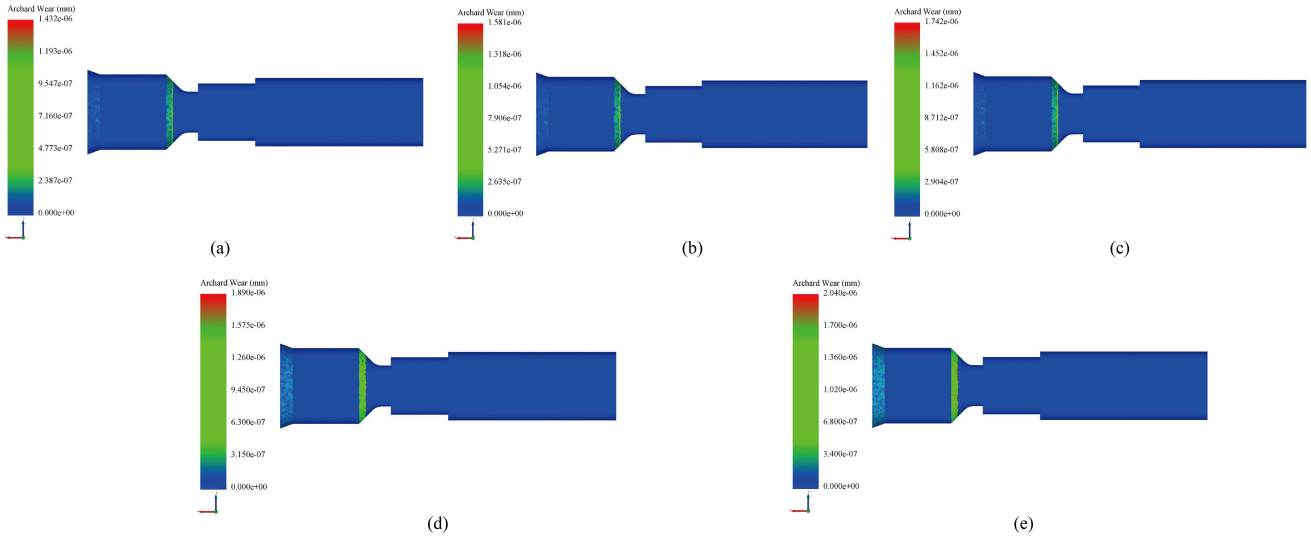

Fig. 13. Erosion cloud map of different mass flow rates: (a) 0.0005 kg/s, (b) 0.001 kg/s, (c) 0.0015 kg/s, (d) 0.002 kg/s and (e) 0.0025 kg/s.

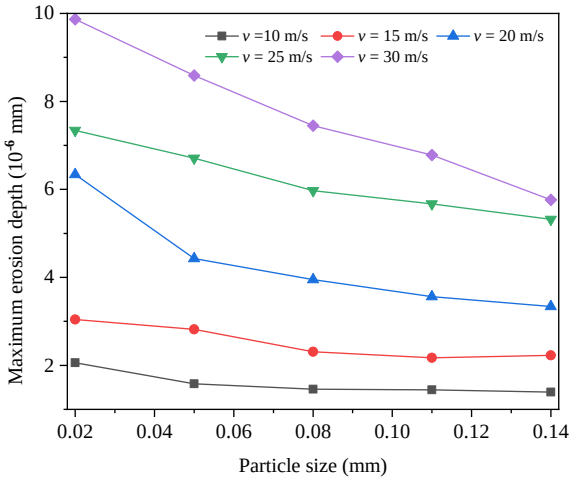

Fig. 14. Maximum erosion depth versus particle size curves.

4.4 Structural optimisation

This study identified key factors that significantly impact valve body erosion, which include fluid velocity, particle diameter, particle morphology, and mass flow rate. To mitigate the erosive damage caused by fluid-borne particles and preserve the integrity of the pressure-retention coring process, as well as the accuracy of subsequent fluid measurements, we optimized the valve body design in erosion-prone areas, as illustrated in Fig. 15. Specifically, the original sharp-corner design was replaced by a smooth-transition one, which reduces the intensity of particle flow impact on the local wall surface. In addition, the flow channel diameter was slightly increased to reduce the flow velocity and alleviate localized pressure gradients, thus further mitigating the erosion risks.

In order to quantitatively assess the wear resistance of the improved valve design, we performed comparative simulations of the original and modified structures using identical flow parameters and boundary conditions. The simulation parameters were set as follows: Particle diameter of 0.05 mm, mass flow rate of 0.0005 kg/s, and fluid velocity of 20 m/s. As illustrated in Fig. 16, the modified structure demonstrated significantly reduced particle velocity and weaker impact forces on the wall surface. As a result, surface erosion in the improved design was substantially reduced, with the maximum erosion depth decreased by 10% and the maximum pressure reduced to 69% of that in the original design. These enhancements not only improved the erosion resistance and sealing performance of the valve but also ensured better adaptability and reliability for engineering applications in complex field environments.

4.5 Field tests

In order to verify the application performance of the improved check valve in actual field conditions, field tests were Nonducted in the Jiang Han Basin in Hubei Province, China. The coring well was a development well located in the Zhong Tan fracture tectonic zone of the Qian Jiang depression in the Jiang Han Basin, with a design depth of 2,749 meters. The site conditions were complex, with target formation pressures ranging from 10 to 25 MPa. Brine-based drilling fluid was used, with a discharge rate of up to 30 L/s. A total of two pressure-preserving coring operations were performed, along with pressure release and gas collection procedures. The two designed check valves successfully achieved downhole sealing without leakage. After completing pressure-preserving coring, the valves seamlessly connected with the follow-up measurement equipment and completed the pressure relief operations without blockage.

5. Conclusions

In this work, to address the technical challenges of internal pressure release and fluid collection following pressure-preserved coring in deep oil and gas wells, a specialized check valve designed for shale gas collection and testing systems has been developed. Both laboratory and field experiments

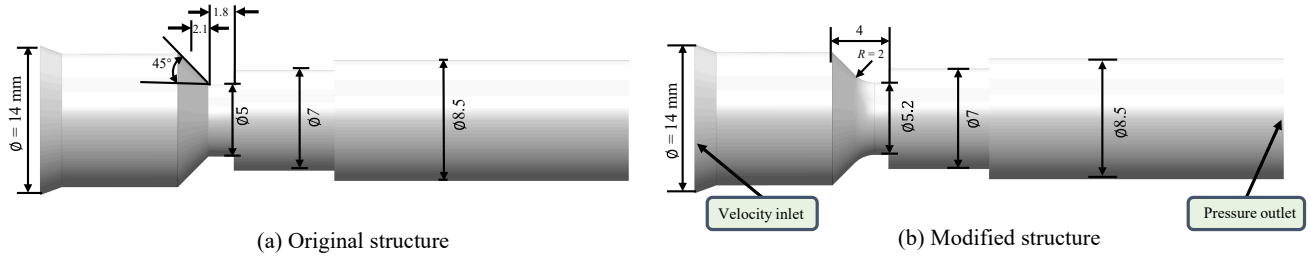

(a) Original structure (b) Modified structure

Fig. 15. Valve body structure optimization.

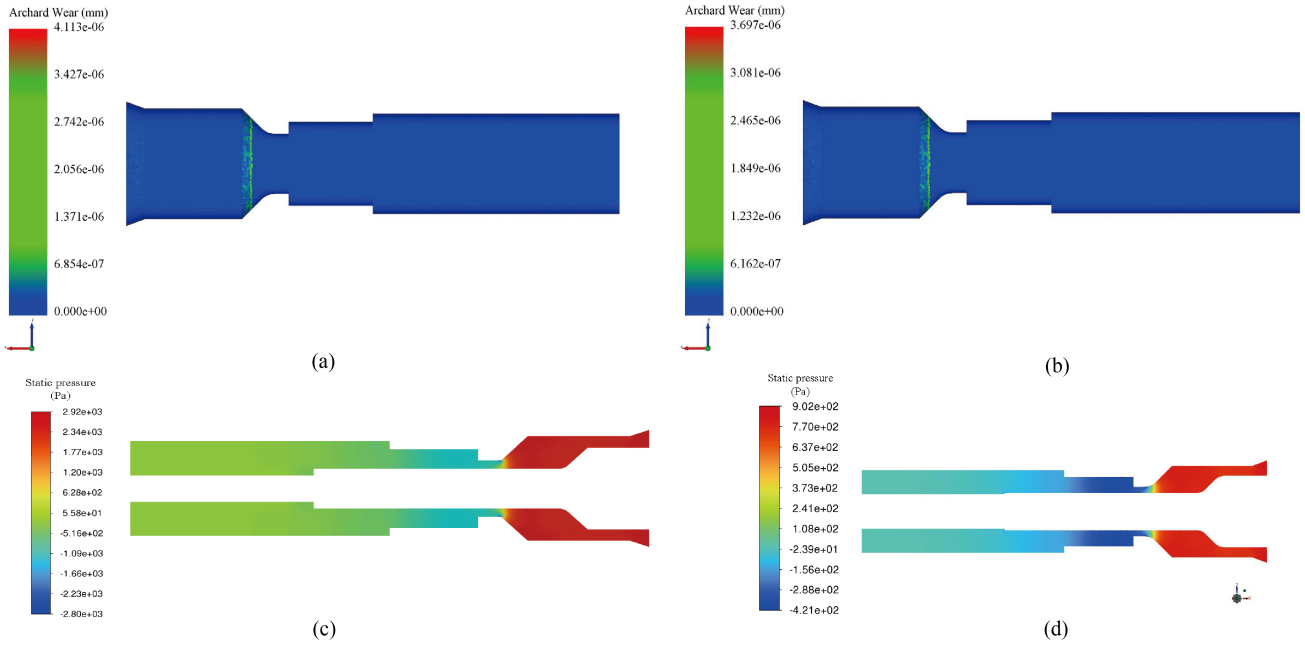

Fig. 16. Comparison of simulation results before and after structural optimization: (a) Erosion depth before optimization, (b) erosion depth after optimization, (c) fluid pressure before optimization and (d) fluid pressure after optimization.

were conducted to assess its field performance to ensure the successful implementation of pressure-preserved coring. Additionally, to prevent valve seal failure due to particle erosion, which could lead to a failure in pressure-preserved coring, numerical simulations of internal erosion within the valve body were performed using the coupled CFD-DEM method. This study explored the influence of particle mass flow rate, fluid velocity, particle shape, and particle size on valve body erosion under actual operating conditions, yielding the following key conclusions:

1) The practical performance of the developed check valve has been validated through both laboratory tests and field trials. It successfully met the 70 MPa sealing requirement for deep oil and gas wells, ensuring efficient pressure relief without blockage, even in complex mud environments. Furthermore, it enables seamless, leak-free integration between the pressure-preserved coring device and the subsequent testing equipment, enabling the smooth continuation of the testing process.
2) By employing coupled CFD-DEM calculations, the motion characteristics of gas-solid two-phase flow inside the valve body were analyzed. The results indicate that in the narrow section of the flow channel inside the valve, fluid velocity increases significantly, generating a negative pressure zone in this regions, which is also the area of most pronounced erosion on the valve body.
3) The shape of particles has a significant impact on valve erosion. Under the same mass and density conditions, non-spherical particles cause greater erosion depth than spherical particles. Furthermore, as particle mass flow rate increases, the maximum erosion depth grows significantly, with this trend being more pronounced under higher mass flow rates. As the inlet velocity increases, the maximum erosion depth also rises noticeably. When the inlet velocity increases from 5 to 25 m/s, the erosion depth increases by a factor of six.
4) The maximum erosion depth decreases as the particle size increases. When the particle size increases from 0.02 to 0.08 mm, a significant reduction in erosion depth is observed, with a tenfold decrease. However, when the particle size exceeds 0.08 mm, the reduction rate in erosion depth slows. Overall, when the particle size increases from 0.02 to 0.14 mm, the erosion depth is reduced by 33%.
5) To prevent seal failure caused by erosion, which could

lead to failure in pressure-preserved coring, the valve body structure was optimized. The results show that the redesigned structure reduces peak pressure by 69% of the original value and significantly reduces the maximum erosion depth.

Acknowledgements

This research was supported by National Key Research and Development Program for Deep Earth (No. 2024ZD1003901), the National Natural Science Foundation of China (Nos. 52304146 and 52104142) and the China Postdoctoral Science Foundation (No. 2023M742460).

Conflict of interest

The authors declare no competing interest.

References

Abid, K., Spagnoli, G., Teodoriu, C., et al. Review of pressure coring systems for offshore gas hydrates research. Underwater Technology, 2015, 33: 19-30.

Alghurabi, A., Mohyaldinn, M., Jufar, S., et al. CFD numerical simulation of standalone sand screen erosion due to gas-sand flow. Journal of Natural Gas Science and Engineering, 2021, 85: 103706.

Archard, J. Contact and rubbing of flat surfaces. Journal of Applied Physics, 1953, 24: 981-988.

Chen, J., Wang, Y., Li, X., et al. Erosion prediction of liquid-particle two-phase flow in pipeline elbows via CFD-DEM coupling method. Powder Technology, 2015, 275: 182-187.

Domagała, M., Momeni, H., Domagala-Fabis, J., et al. Simulation of particle erosion in a hydraulic valve. Materials Research Proceedings, 2018, 5: 17-24.

Duarte, C. A. R., de Souza, F. J., dos Santos, V. F. Mitigating elbow erosion with a vortex chamber. Powder Technology, 2016, 288: 6-25.

Fang, X., Zhang, C., Li, C., et al. Structural design and numerical analysis of an all-metal screw motor for drilling applications in high-temperature and high-pressure environments in ultra-deep wells. Applied Sciences, 2023, 13: 8630.

Farokhipour, A., Mansoori, Z., Rasteh, A., et al. Study of erosion prediction of turbulent gas-solid flow in plugged tees via CFD-DEM. Powder Technology, 2019, 352: 136-150.

Fry, A., Lovelock, P., Smith, N., et al. An innovative high temperature solid particulate erosion testing system. Wear, 2017, 376: 458-467.

Gao, M., Chen, L., Fan, D., et al. Principle and technology of coring with *in-situ* pressure and gas maintaining in deep coal mine. Journal of China Coal Society, 2021, 46(3): 885-897. (in Chinese)

Guo, D., Li, J., Wang, D., et al. Structural improvement of differential motion assembly in *in situ* pressure-preserved coring system using CFD simulation. Applied Sciences, 2023, 13: 4108.

Haider, A., Levenspiel, O. Drag coefficient and terminal velocity of spherical and nonspherical particles. Powder Technology, 1989, 58: 63-70.

Hu, Y., Xie, J., Xue, S., et al. Research and application of thermal insulation effect of natural gas hydrate freezing corer based on the wireline-coring principle. Petroleum Science, 2022, 19: 1291-1304.

Kong, L., Xie, H., Li, C. Coupled microplane and micromechanics model for describing the damage and plasticity evolution of quasi-brittle material. International Journal of Plasticity, 2023, 162: 103549.

Lisowski, E., Filo, G. CFD analysis of the characteristics of a proportional flow control valve with an innovative opening shape. Energy Conversion and Management, 2016, 123: 15-28.

Liu, E., Huang, S., Tian, D., et al. Experimental and numerical simulation study on the erosion behavior of the elbow of gathering pipeline in shale gas field. Petroleum Science, 2023, 21: 1257-1274.

Lyu, C., Chen, X., Liu, Y., et al. Simulation analysis and prevention and control measures of elbow erosion of natural gas transportation pipeline based on fluent. Welded Pipe and Tube, 2023, 46(1): 13-18. (in Chinese)

Oesterlé, B., Dinh, T. B. Experiments on the lift of a spinning sphere in a range of intermediate Reynolds numbers. Experiments in Fluids, 1998, 25: 16-22.

Priest, J. A., Druce, M., Roberts, J., et al. PCATS Triaxial: A new geotechnical apparatus for characterizing pressure cores from the Nankai Trough, Japan. Marine and Petroleum Geology, 2015, 66: 460-470.

Quan, J., Liu, X., Wang, C., et al. A study on corrosion failure of the circulation line with valve openings in atmospheric tower based on CFD. Engineering Failure Analysis, 2022, 141: 106633.

Shen, W., Li, X., Ma, T., et al. High-pressure methane adsorption behavior on deep shales: Experiments and modeling. Physics of Fluids, 2021, 33: 063103.

Shi, X., Xie, H., Li, C., et al. Influence of the mechanical properties of materials on the ultimate pressure-bearing capability of a pressure-preserving controller. Petroleum Science, 2024a, 21(5): 3558-3574.

Shi, X., Xie, H., Li, C., et al. Performance of a deep *in situ* pressure-preserving coring controller in a high-temperature and ultrahigh-pressure test system. Journal of Rock Mechanics and Geotechnical Engineering, 2024b, in press, https://doi.org/10.1016/j.jrmge.2024.01.012.

Simic, M., Herakovic, N. Reduction of the flow forces in a small hydraulic seat valve as alternative approach to improve the valve characteristics. Energy Conversion and Management, 2015, 89: 708-718.

Xie, H., Gao, F., Ju, Y., et al. Novel idea and disruptive technologies for the exploration and research of deep earth. Advanced Engineering Sciences, 2017, 49(1): 1-8. (in Chinese)

Xie, H., Liu, T., Gao, M., et al. Research on *in-situ* condition

preserved coring and testing systems. Petroleum Science, 2021, 18: 1840-1859.

Xu, L., Zhang, Q., Zheng, J., et al. Numerical prediction of erosion in elbow based on CFD-DEM simulation. Powder Technology, 2016, 302: 236-246.

Yang, S., Fan, J., Zhang, L., et al. Performance prediction of erosion in elbows for slurry flow under high internal pressure. Tribology International, 2021, 157: 106879.

Yang, X., Li, S., Yang, B., et al. Influence of Valve Core and Seat Structure of Overflow Valve on Flow Field Performance and Optimization Design. IOP Conference Series: Earth and Environmental Science, 2018, 170: 022112.

Ye, Y., Yin, C., Li, X., et al. Effects of groove shape of notch on the flow characteristics of spool valve. Energy Conversion and Management, 2014, 86: 1091-1101.

Yin, Y., Yuan, J., Guo, S. Numerical study of solid particle erosion in hydraulic spool valves. Wear, 2017, 392: 174-189.

Zhang, J., Shi, M., Wang, D., et al. Fields and directions for shale gas exploration in China. Natural Gas Industry B, 2022, 9: 20-32.

Zhang, Y., Reuterfors, E. P., McLaury, B. S., et al. Comparison of computed and measured particle velocities and erosion in water and air flows. Wear, 2007, 263: 330-338.

Zhou, S., Zhang, J., Zou, C., et al. A new method for testing shale gas content based on pressure-holding coring technology. Journal of China Coal Society, 2022, 47(4): 1637-1646. (in Chinese)

Zhu, H., Zhou, Z., Yang, R., et al. Discrete particle simulation of particulate systems: Theoretical developments. Chemical Engineering Science, 2007, 62: 3378-3396.